Sensors & Actuators: A. Physical 350 (2023) 114121

Contents lists available at ScienceDirect

Sensors and Actuators: A. Physical

journal homepage: www.journals.elsevier.com/sensors-and-actuators-a-physical

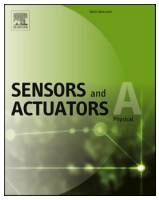

A droplet-based micropillar-enhanced acoustic wave (μPAW) device for viscosity measurement

Ilia Chiniforooshan Esfahani, Hongwei Sun *

Mechanical and Industrial Engineering Northeastern University, Boston, MA 02115, USA

ARTICLE INFO

Keywords:
Quartz crystal microbalance (QCM)
Micropillars
Equivalent circuit
Viscosity

ABSTRACT

Viscosity monitoring has recently received significant attention in various fields such as pharmacy, oil industry, food industry, and medical diagnostics. Given that the commercially available viscometers usually require a large sample volume to conduct accurate measurement, there is an urgent need to develop a viscometer that can consume the least sample while maintaining high accuracy. Despite of being simple, rapid, and cost-effective, quartz crystal microbalance (QCM) based viscometers are low in sensitivity and not able to measure viscosity directly. This work focuses on the development of a novel micropillar-enhanced QCM viscosity measurement device which relies on the coupled vibration between micropillars and quartz substrate (QCM-P) to achieve an ultra-sensitive viscosity measurement of a sample droplet. A hybrid model by integrating an equivalent circuit and numerical simulation approach was established to understand the working principle of the QCM-P device and evaluate the viscosity value. The experimental results and analysis demonstrate that the micropillar-enhanced acoustic wave (μPAW) devices such as QCM-P viscometer is a promising device for droplet-based viscosity measurement.

1. Introduction

Viscosity monitoring is becoming increasingly important in various fields such as in food industry for quality control [1], oil industry for observing the deterioration of engine oil [2], pharmacy to ensure the miscibility of drugs and blood [3], and biomedical diagnostics for analyzing the biofluids (e.g., saliva and urine) [4–6]. Conventional viscometers are typically categorized into four types including tube-type capillary or orifice viscometers [7], falling-body viscometers [8], rotational viscometers [9], and vibrational viscometers [10]. The orifice and falling-body viscometers evaluate the viscosity by measuring the timing of fluid or falling object. The working principle of rotational and vibrational viscometers are based on the measurement of the applied force at various shear rates. Although conventional viscometers exhibit high precision in viscosity measurement, they typically require a large sample volume to obtain reliable and accurate results. Thus, developing a rapid and cost-efficient device capable of measuring viscosity with a very low sample consumption is of great importance to meet the needs.

Acoustic wave (AW) devices such as quartz crystal microbalance (QCM) sensors have become increasingly popular as mass sensors in a wide range of applications such as environmental monitoring for detecting harmful gases [11], food industry for detecting preservatives in beverages [12], and pharmaceutical industry for drug analysis [13]. The AW-based detection method is featured as being simple, rapid, and cost-effective [14]. Among the AW devices, QCM has gained increasing attention in recent years due to their high sensitivity, specificity, and resolution [15]. For example, QCM composed of colloidal phenyl-terminated carbon nitride (Ph-g-C3N4) nanoflakes was utilized for the rapid detection of formic acid (HCOOH) [17] and achieved the limit of detection (LOD) of 80 ppb. Recently, a comprehensive overview of QCM coated with nanoporous materials for chemical vapors detection methods have been performed by Torad et al. [18]. Generally, a QCM device is made of an AT-cut quartz disk with gold electrodes fabricated on both sides. When an alternating current (AC) voltage is applied to the electrodes, the quartz substrate shows mechanical deformation due to the so-called piezoelectric effect and undergoes a thickness-shear mode oscillation at the resonance frequency, f_o, based on its crystal orientation [16]. In addition to mass sensing detection, QCM devices have been utilized for viscosity measurement [19]. When QCM operates in liquid, part of the shear vibration is transmitted to the liquid resulting in elastic energy dissipation [20]. The interaction between the quartz and the surrounding fluid leads to a damping effect on the elastic shear waves at

* Corresponding author.
E-mail address: ho.sun@northeastern.edu (H. Sun).

https://doi.org/10.1016/j.sna.2022.114121
Received 5 September 2022; Received in revised form 26 November 2022; Accepted 22 December 2022
Available online 24 December 2022

the liquid interface that causes a frequency shift. By taking advantage of small load approximation (SLA), the resonance frequency shift, Δf, and half bandwidth (HBW) shift, ΔΓ, of the QCM operating in a fluid medium are related to viscosity by the following equations [21–24]:

$$\Delta f = -\frac{f_0^{3/2}}{Z_q}\sqrt{\frac{\rho_L \mu_L}{\pi}} \tag{1a}$$

$$\Delta \Gamma = \frac{f_0^{3/2}}{Z_q}\sqrt{\frac{\rho_L \mu_L}{\pi}} \tag{1b}$$

where ρ_L is the density and μ_L is the viscosity of the fluid and Z_q is the quartz characteristic impedance (8.8×10^6 kg m^{-2} s^{-1}). On the other hand, the disadvantages of using QCMs for viscosity measurement include: a) a relatively low sensitivity and b) the inability to obtain liquid viscosity directly as the response of QCM depends on both the density and viscosity of the solution [25]. Approaches for separating the viscosity and density effects in the QCM measurement have been studied, including the use of dual QCMs and reference crystals [26,27]. Another one is the use of two QCM sensors: one with a smooth surface and the other with a textured surface where the trapped liquid in the textured surface behaves as a pure mass loading, and a comparison with the smooth surface can provide information about the density of the solution [28]. Tan et al. developed a theoretical framework to separate the density and viscosity from the measurement of QCM [29].

Recently, a novel mass sensing mechanism has been identified by attaching polymer micropillars on acoustic wave devices including QCM surface (QCM-P), which exhibited significantly improved sensitivity over conventional QCM [30,31]. The QCM-P system can be modeled as a two-degree-of-freedom system with the QCM as the main resonator and the micropillar as the second resonator [32]. In another study, the dynamic characteristics of QCM-P were analyzed using an equivalent circuit model based on the Krim-Holtz-Leedom-Matthaei (KLM) [33]. Despite its prediction capability, this model suffers from the limitation that it can only be used for circular-shaped micropillars in an inviscid solution. To the best of our knowledge, no analytical relation has been provided for the hydrodynamic loading on square micropillars of finite thickness [34].

This research reports the development of a novel droplet-based viscosity measurement method using a QCM-P device, which is capable of measuring liquid viscosity with high sensitivity and a small sample volume (200 μl). The fabrication procedure of micropillars on QCM substrate is introduced first. Then the experimental setup for measuring the liquid viscosity and the responses of QCM-P sensors to sucrose droplets (aq) with concentrations ranging from c = 10–40 wt% are reported. A novel integrative equivalent circuit and numerical simulation model is developed to analyze the dynamics of QCM-P in a viscous liquid solution and calculate its viscosity.

2. Experimental and modeling methodologies

2.1. Preparation of QCM-P

Commercial QCMs (10 MHz, Fortiming Corp., MA) with both sides coated with 100 nm-thickness gold film and a sensing area of 5.11 cm^2 were utilized in this research. The QCM-P sensors were prepared by directly fabricating polymethyl methacrylate (PMMA) micropillars on the surface of QCMs via a thermal nanoimprinting lithography process (T-NIL) in four sequential steps (see Fig. 1):

Step A: Preparation of SU-8 mother mold by UV photolithography. The micropillars were fabricated with a SU-8 3000 series photoresist (MicroChem Corp., Newton, MA) in a standard UV photolithography process; Step B: Preparation of Polydimethylsiloxane (PDMS) stamp by soft lithography. The micro-holes within the PDMS stamp exactly match the geometry of SU-8 micropillars in the mother mold; Step C: Fill the PDMS mold with a PMMA solution. PMMA solution was filled into the PDMS microholes via a spin-coating process; Step D: Fabrication of micropillars on the QCM using T-NIL. The micropillars which are arranged in a square lattice pattern completely cover the sensing area. The details of fabricating micropillars on the QCM surface can be found somewhere else [30]. Two types of micropillars were fabricated on the surface, including square micropillars with a center-to-center distance of 21 μm and a side of 10 μm, and heights of h_p = 6.4, 10.3, 11.5, 13.9 and 18.1 μm and circular micropillars with a center-to-center distance of 16 μm and diameter of 5 μm, and height of h_p = 8.3, 9.2, 10.8, and 12.3 μm, respectively. The total pillar number of squared micropillar QCM-P is around 1.15×10^6 while for circular micropillar QCM-P around 1.99×10^6. As a comparison, a conventional PMMA film-based QCM (QCM-F) with a thickness of ~3 μm was fabricated. It should be aware that the QCM-F has the same sensitivity as the traditional bare QCM since the acoustic phase shift, ϕ of PMMA film is small (~ 0.15) [35].

2.2. Experimental setup and procedure

The experimental setup for evaluating the characteristics of QCM-P is shown in Fig. 2. It consists of a QCM-P sensor holder, co-axial cable (50 Ω) network analyzer (Agilent Technologies, HP8753D), data acquisition system (DAQ), and PC. During each experiment, a drop of 200 μl solution was gently loaded on the QCM-P and QCM-F sensors using a pipette until the solution completely covered the QCM-P sensing area. The network analyzer (Agilent Technologies, HP8753D) measured the conductance spectrum ($Re(1/Z) vs\, f$) of the sensors, and the signal was analyzed on a personal computer through a built-in LabVIEW program (National Instruments). Finally, the Lorentzian curve fitting method was applied to the measured conductance spectrum and extract the HBW, $\Delta\Gamma$, and resonance frequency, f_0, of the devices [36].

To establish a baseline, a control experiment was conducted using

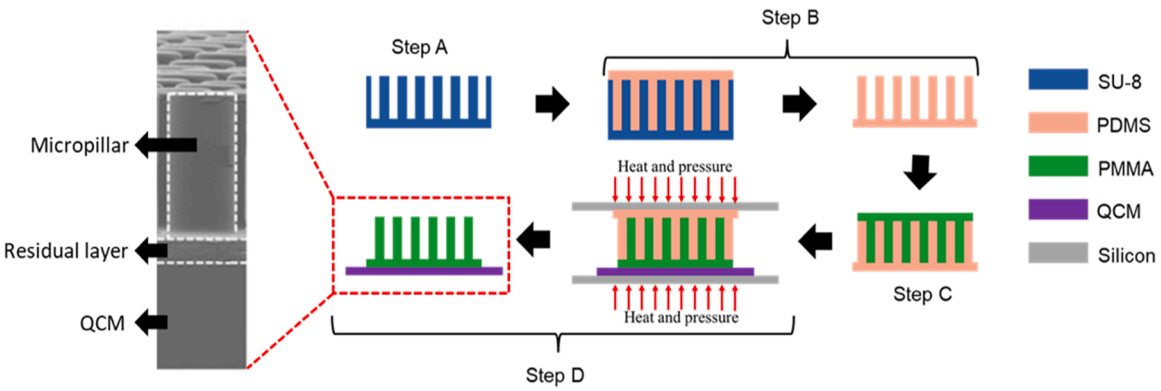

Fig. 1. Flowchart of fabricating QCM-P sensors using T- NIL.

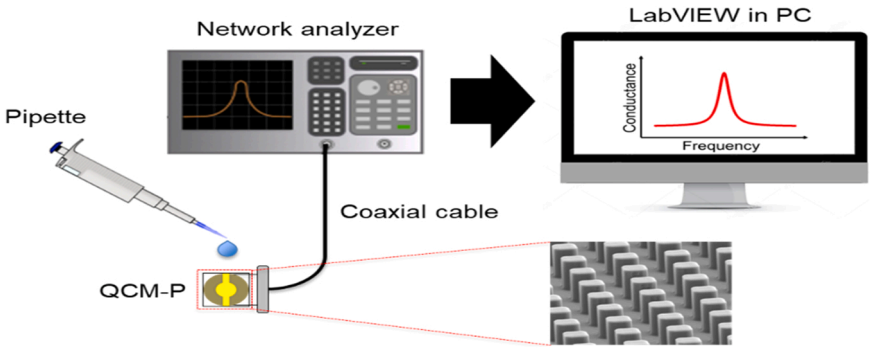

Fig. 2. Schematic of the QCM-P measurement system using a network analyzer.

deionized (DI) water first. After that, the measurements were repeated by depositing the droplets of sucrose solution (aq) with concentrations ranging from $c = 10$–40 wt%. The sucrose solutions (aq) were prepared by dissolving sucrose powder (Alden Corp., NY) in DI water, followed by stirring at 60 °C for 30 min and cooled to room temperature. The effect of solution properties on the QCM-P was observed by monitoring the shifts in resonance frequency (Δf) and HBW ($\Delta \Gamma$) from the baseline values. It should be noted that the absolute values of Δf and $\Delta \Gamma$ are presented in the research and all the experiments were repeated three times to ensure the reproducibility of the results.

2.3. Modeling methodology

The equivalent circuit models have been widely used to investigate the response of QCM due to their simplicity [37], including Mason's model [38], the Butterworth-Van Dyke (BVD) model [39], and the Krimholtz-Leedom-Matthaei (KLM) model [40]. These models consist of different compositions of electrical parameters such as resistance, capacitance, and inductance. The goal is to find the circuit's impedance (Z) from the load impedance (Z_L) on the quartz surface with respect to the frequency (f or ω). The impedance of the QCM in the KLM model is expressed as [41]:

$$Z = \frac{1}{i\omega C_0}\left[1 - \frac{K^2}{\xi_q h_q}\frac{2\tan(\xi_q h_q/2) - i(Z_L/Z_q)}{1 - i(Z_L/Z_q)\cot(\xi_q h_q)}\right] \tag{2}$$

Where

$$\xi_q = \omega\sqrt{\rho_q/c_q}, Z_q = \sqrt{\rho_q c_q}, c_q = c_{66} + \frac{e_{26}^2}{\varepsilon_{22}} + i\omega\eta_q$$

C_0 is the static capacitance, K is the electromechanical coupling factor, Z_q is the quartz characteristic impedance, ρ_q is the mass density, e_{26} is the piezoelectric constant, ε_{22} is the permittivity, c_{66} is the shear modulus, and η_q is the viscosity of the AT-cut quartz.

It is assumed that the quartz plate has a harmonic displacement in the y-direction with an amplitude of u_0 and the displacements in other directions are negligible due to the sensors operating in the thickness-shear mode (Fig. 3). As a result, the load impedance on the quartz substrate can be evaluated by [41]:

$$Z_L = \frac{\hat{\tau}_0}{v_0} \tag{3}$$

Where v_0 and $\hat{\tau}_0$are the velocity and shear stress of the upper surface of the QCM sensor.

Previous studies show that the load impedance of circular micropillars on the quartz surface can be evaluated by solving Newton's second law and Euler-Bernoulli beam equations, while it is challenging to evaluate the hydrodynamic loading on rectangular micropillars with finite thickness [34]. Thus, a 3D numerical simulation based on the aeroacoustics-structure interaction (AeSI) was used to assist in the calculation of the shear stress ($\hat{\tau}_0$) or load impedance (Z_L) of micropillars in viscous solutions. The simulation was performed on the commercial COMSOL software (COMSOL, Inc., MA). The unit cell was divided into four subdomains: PMMA film (plane-strain), PMMA micropillar (plane-strain), surrounding solution (aeroacoustics), and perfectly match layer (PML), as seen in Fig. 4 with applied boundary conditions in each domain. The shear wave propagation in micropillars and residual layers is described by the equation of shear displacement in structural mechanics [42]. A PML is used to simulate the absorption of acoustic waves within a numerical domain since the thickness of the far-field acoustic domain is much larger than the micropillar height. The details of the simulation geometry, meshing, and boundary conditions can be found in the Supplementary materials.

Linearized Navier Stokes (LNS) equations have been used previously to determine acoustic waves in the domain where viscous effects act as a non-negligible role [43,44]. To solve the LNS equations, the flow variables, such as velocity, are assumed to be the combination of a time-independent mean flow and unknown time-dependent perturbations. As a result, the Navier Stokes equations in the frequency domain are simplified as [45]:

$$-i\omega\hat{\rho} + \nabla(\rho_0\hat{u} + \hat{\rho}u_0) = 0 \tag{7a}$$

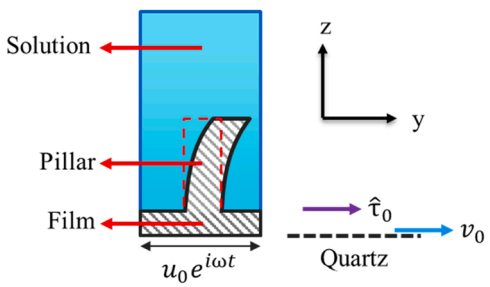

Fig. 3. Continuity condition at the interface of quartz and micropillar.

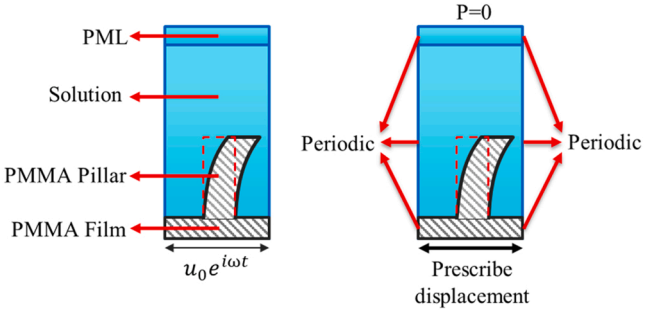

Fig. 4. Subdomains and boundary conditions of the unit cell of micropillar.

$$\rho_0[-i\omega\hat{u}+(\hat{u}\bullet\nabla)u_0+(u_0\bullet\nabla)\hat{u}]+\hat{\rho}(u_0\bullet\nabla)u_0=\nabla\sigma+F-u_0M \quad (7b)$$

u and ρ represent velocity and density, respectively. M and F represent mass and force source terms. The mean components of the flow variables are denoted by subscript zero, and the perturbed component with the symbol ˆ above the variable. The mean flow component is assumed to be independent of time. The perturbation components are derived from the steady-state conditions. For example, any perturbated quantity q' is expressed as:

$$q'(x,t)=\mathrm{Re}\{\hat{q}(x)e^{-i\omega t}\} \quad (8)$$

where $\hat{q}$ is a complex quantity and ω is the angular frequency. The fluid at the solid-liquid interface experiences the no-slip boundary condition expressed as:

$$u_{t,fluid}=\frac{\partial u_{solid}}{\partial t}=-i\omega u_{solid} \quad (9)$$

$u_{t,fluid}$ and u_{solid} are denoted as the velocity of liquid and displacement of solid at the solid-liquid interface, respectively. It is worth noting that the vibrating micropillar driven by the QCM is the source of the acoustic waves, and there exists a unique coupling between the micropillar shear displacements and the fluid acoustic field.

3. Results and discussion

3.1. Model validation

A mesh independence study was conducted to ensure a reliable solution. The mesh independence analysis of the simulation was performed for the squared micropillar QCM-P with $h_p = 18$ μm by refining the degree-of-freedom (DOF). Fig. 5 presents the shear stress at the quartz top surface. It is apparent that the results become stable after the DOF number reaches 500,000, which is used for the rest of the simulations.

To validate the model, a series of experiments were conducted using QCM-F for sucrose solutions (aq) with concentrations ranging from $c = 0$ (DI water) to 40 wt%, and the Δf and $\Delta\Gamma$ were compared with those predicted by SLA theoretical model (Eqs. 1a and 1b) and the developed hybrid model (Fig. 6). The values of viscosity and density of sucrose solutions corresponding to different concentrations are reported in Table 1. As can be seen in Fig. 6, Δf and $\Delta\Gamma$ increase linearly with the increase of $\sqrt{\rho\eta}$, which is consistent with the SLA theoretical model. Notice that there is a slight deviation between the prediction of the SLA model and measurement due to simplifying assumptions in calculating the load impedance in SLA model. But the hybrid model accurately

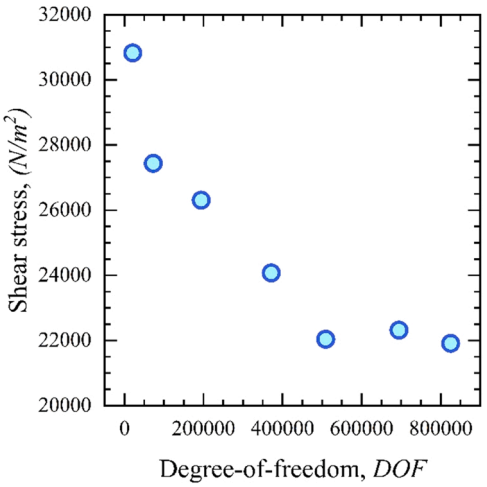

Fig. 5. Mesh independence study of the simulation.

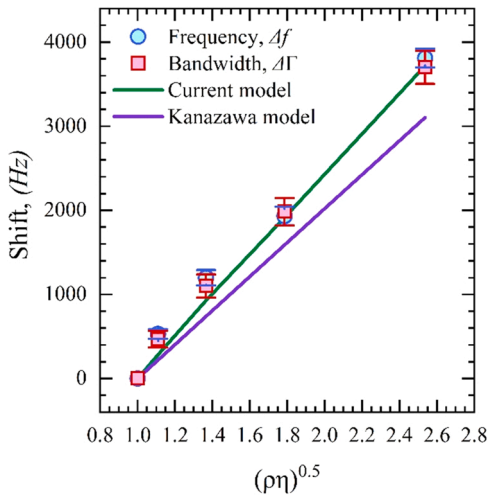

Fig. 6. Comparison of experimental measurements for sucrose solution (aq) with the prediction of Kanazawa model (Eqs. 1a and 1b) and the hybrid model.

Table 1
The viscosity and density of sucrose solution.

Concentration (wt%)	Viscosity (cP)	Density (kg/m^3)
10	1.186	1038
20	1.727	1081
30	2.831	1127
40	5.474	1176
50	13.706	1230

predicts the linear relationship of the frequency shift Δf and HBW $\Delta\Gamma$ with concentration.

The f_0 and Γ predicted by the model were compared with the experimental results for QCM-P in the DI water (Fig. 9). The model successfully captured nonlinear responses of f_0 and Γ with respect to h_p. As h_p increases, the f_0 of QCM-P decreases, which is consistent with the Sauerbrey theory. A sudden "drop and jump" was observed in the f_0 when the h_p reaches the so-called "critical height" due to the coupling between the micropillars, resonator, and the solution. The model predicted that the Γ of QCM-P increases with the increase in h_p. It reaches its maximum value at the respective critical height of the micropillar, and then it begins to decrease. The results show that the maximum energy dissipation of the QCM-P occurs near their respective critical heights, which is consistent with experimental measurements and prediction results shown below. The critical heights of square and circular micropillar QCM-P sensors in water are predicted to be 13.5 μm (Figs. 7A) and 9.8 μm (Fig. 7B).

3.2. QCM-P responses in viscous solution

Fig. 8 reports the comparison of the measured $\Delta\Gamma$ and Δf of the sensor with the model prediction results. A good agreement was obtained between the model prediction and experimental observations at different sucrose concentrations. As c increases from 0 (DI water) to 40 wt%, an increasing hydrodynamic loading is imposed on the micropillar structure, resulting in a higher Δf and $\Delta\Gamma$. Fig. 8A shows that the maximum Δf for square micropillar QCM-P was 81 kHz, while the maximum Δf for QCM-F was only 3.8 kHz. According to Fig. 8B, QCM-F had a maximum $\Delta\Gamma$ of 3.7 kHz at $c = 40$ wt%, whereas the $\Delta\Gamma$ of square micropillar QCM-P increased considerably to 82 kHz as the h_p approached critical height ($h_p = 11.5$ μm). Apparently, the square micropillar QCM-P sensors demonstrate higher sensitivity to the changes of viscosity than the QCM-F.

Fig. 9 compares Δf and $\Delta\Gamma$ predicted by the model to those observed

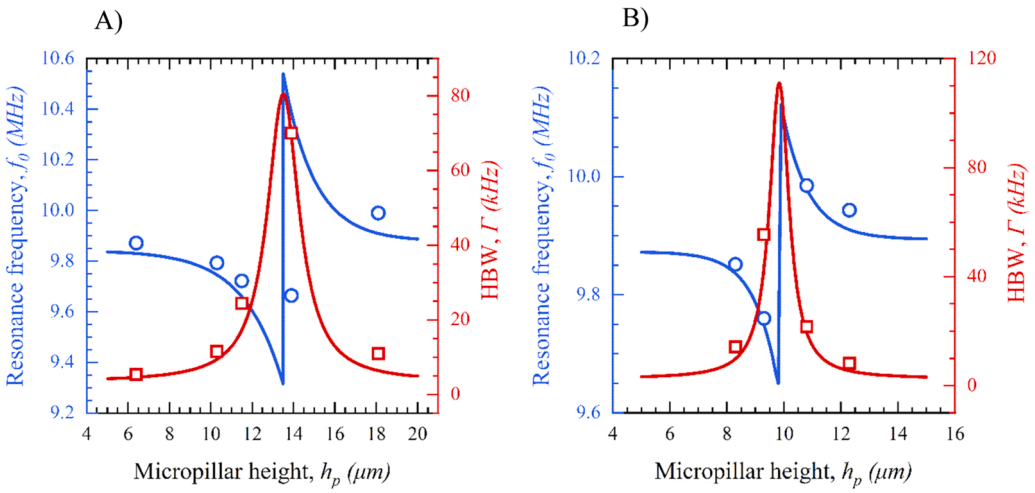

Fig. 7. Model prediction of the resonance frequency, f_0, and HBW, Γ, of the square (A) and circular (B) micropillar QCM-P in the DI water vs. the measured values.

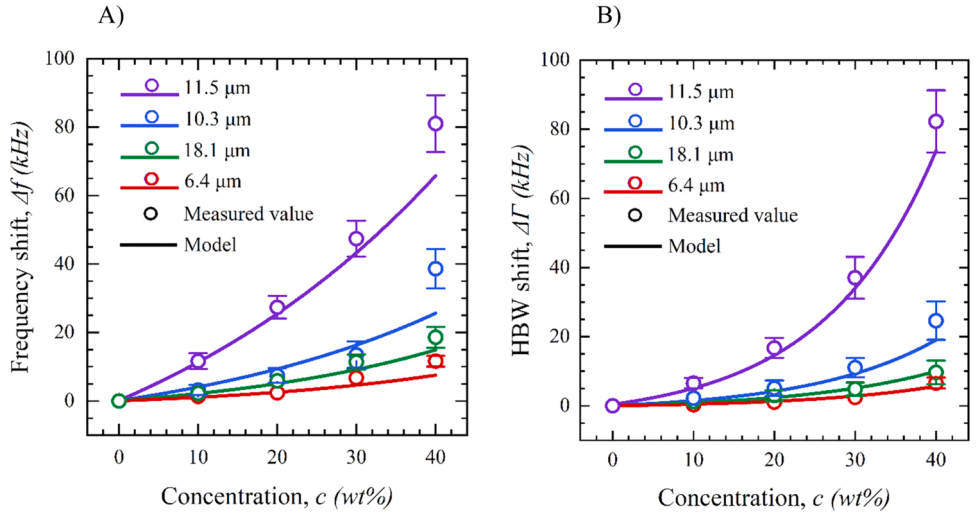

Fig. 8. Model prediction of the frequency shift, Δf, (A) and HBW shift, $\Delta\Gamma$, (B) of square micropillar QCM-P in sucrose solution (aq) vs. the measured values.

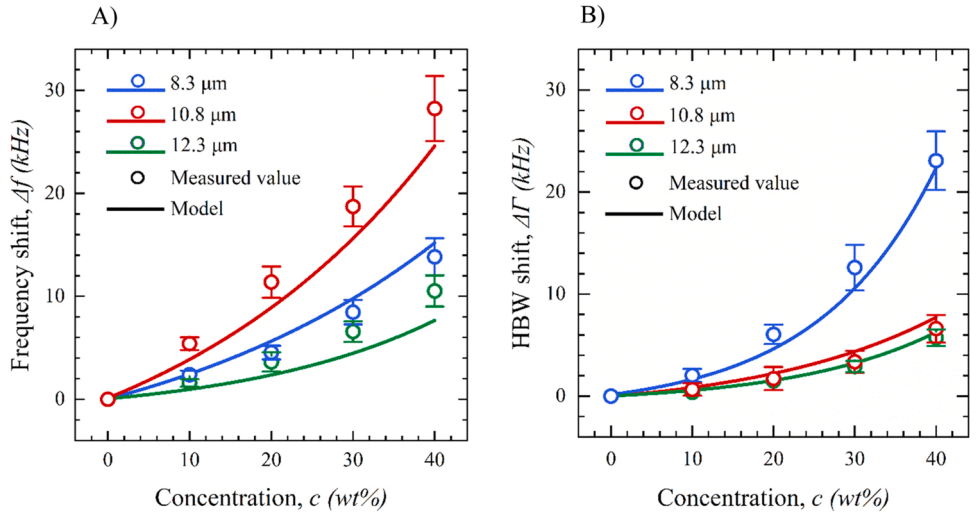

Fig. 9. Model prediction of the frequency shift, Δf, (A) and HBW shift, $\Delta\Gamma$, (B) of circular micropillar QCM-P in sucrose solution (aq) vs. the measured values.

by the circular micropillar QCM-P. It can be seen that the circular micropillar QCM-P sensors behave differently from the square ones. At micropillar height of $h_p = 10.8$ μm, the Δf of the sensor reached 28 kHz while the $\Delta\Gamma$ was only 6.5 kHz for $c = 40$ wt%. However, the QCM-P sensor with $h_p = 8.3$ μm showed a different trend: the $\Delta\Gamma$ of the sensor was around 23 kHz in comparison to 14 kHz for Δf. In addition, Figs. 8–9 show that the highly concentrated solutions result in more shifts in frequency Δf and bandwidth $\Delta\Gamma$, which indicates higher load impedance on the quartz surface.

The Δf and $\Delta\Gamma$ of the QCM-P and QCM-F sensors were evaluated based on the load impedance of QCMs, which is a complex number and calculated using simulation. The real part of the load impedance (Z_L^{re}) corresponds to the Γ, and the imaginary part (Z_L^{imag}) to the f_0. Fig. 10 presents the simulation results for the changes in the real and imaginary parts of the load impedance (ΔZ_L^{re} and ΔZ_L^{imag}) acting on the quartz surface for square and circular micropillars in sucrose solution (aq) with concentrations ranging from $c = 0$ (DI water) to 40 wt%. The results show that as c increases, the ΔZ_L^{re} and ΔZ_L^{imag} increase. In addition, all the QCM-P sensors show higher changes in Z_L^{re} and Z_L^{imag} compared to conventional QCM-F, indicating enhanced sensor responses to property changes. However, due to the limited interactions between the solution and QCM surface, QCM-F is much less sensitive to the variation in the solution properties.

It is proposed that the ratio of $\Delta\Gamma$ to Δf ("DF ratio") can be used to characterize the sensitivity characteristics of the QCM-based sensor. The DF ratio higher than one indicates the $\Delta\Gamma$ is more sensitive to the viscosity change than the Δf, while the DF ratio less than one means the Δf is more sensitive for viscosity measurement. According to the SLA model (Eqs. 1a and 1b), the DF ratio of traditional QCM or QCM-F in a liquid medium equals one, implying Δf and $\Delta\Gamma$ are equally sensitive to the viscosity change. Fig. 11 shows the DF ratio of QCM-P sensors for sucrose solutions (aq) with concentrations of $c = 10$ and 40 wt%. As can be seen, a good agreement was obtained between the model prediction and experimental measurements. Both the model and measured values indicated that the QCM-P sensors represent different sensitivity to Δf and $\Delta\Gamma$.

The results illustrate that the DF ratio increases with the increase of h_p, reaching a maximum value at a critical height. A sudden " jump and drop " behavior is observed near the critical height where the DF ratio reaches a minimum value, typically less than one. It is also worth noting that as the solution concentration increases from $c = 10$–40 wt%, the DF ratio increases, implying a more pronounced impact of solution properties on $\Delta\Gamma$ than Δf. It is concluded that both the HBW shift, $\Delta\Gamma$, and frequency shift, Δf, can be employed for detecting variations in the solution properties. The QCM-P sensors show higher sensitivity to $\Delta\Gamma$ or Δf, depending on the micropillar's characteristics and solution properties. The $\Delta\Gamma$ of QCM-P sensors is more sensitive when the micropillar heights are less than the critical height (13 μm for square micropillars and 9.8 μm for circular micropillars), while the Δf becomes more pronounced when the micropillar heights are greater than the critical height.

Although QCM-P sensors show significant changes in Γ to f in response to liquid property variations, the QCM-based devices can not

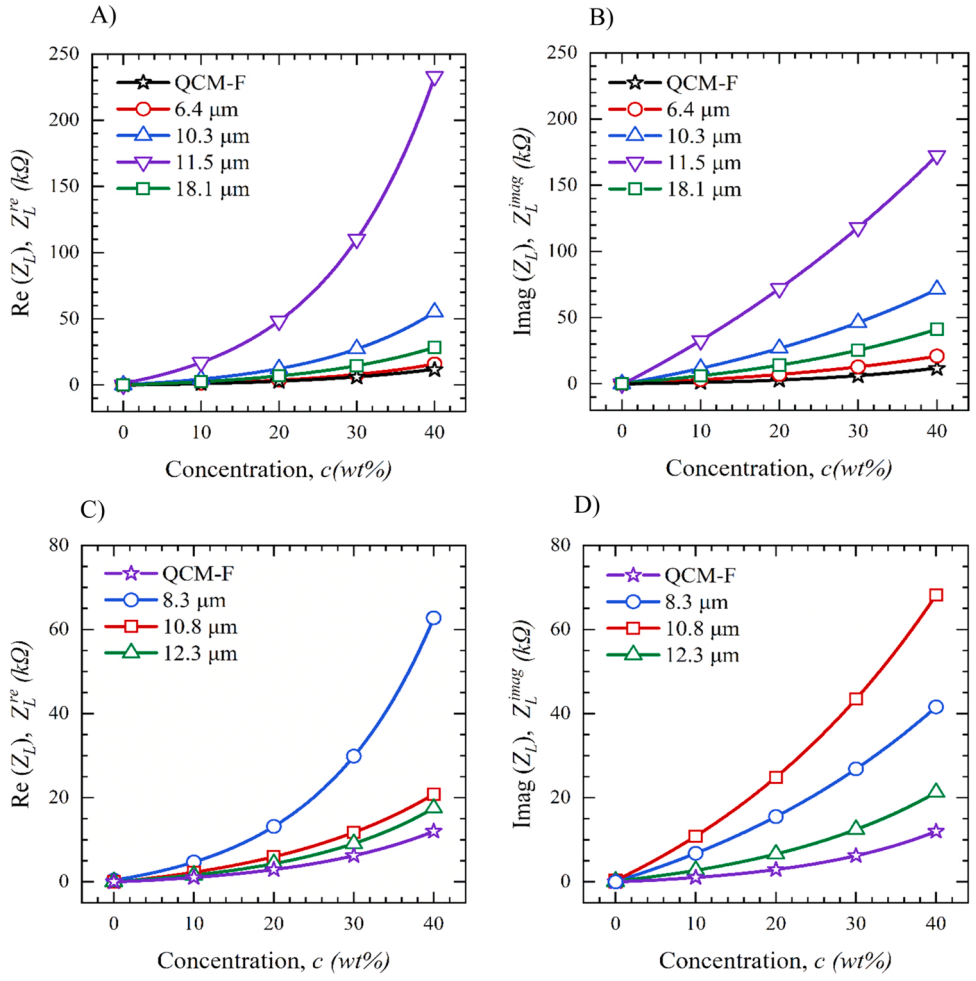

Fig. 10. Simulation results for shift of the real and imaginary parts of load impedance for square (A, B) and circular (C, D) micropillars QCM-P in sucrose solution (aq).

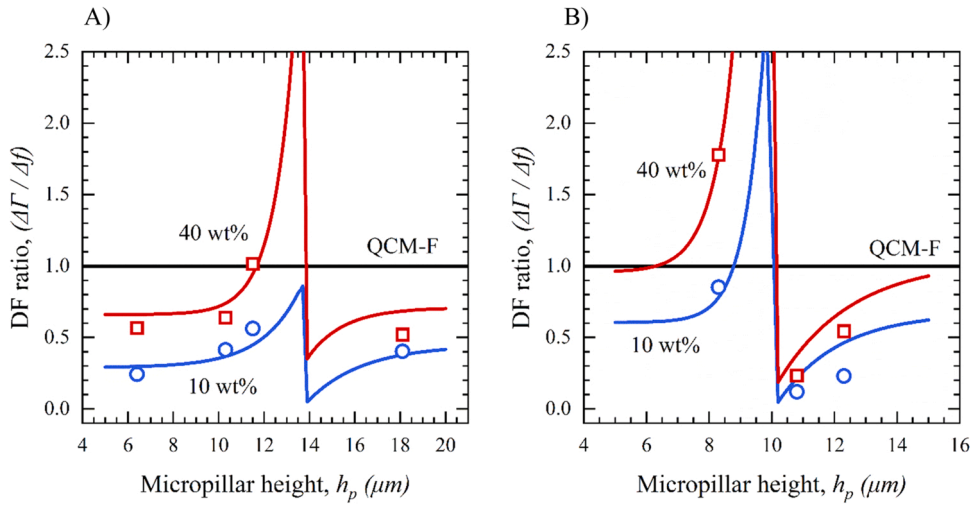

Fig. 11. Predicted DF ratio, ΔΓ/Δf, for sucrose solution (aq) at concentrations of c = 10 and 40 wt% for the square (A) and circular (B) micropillar QCM-P vs. measured values.

directly measure the liquid viscosity as the QCM response depends on both the density and viscosity of the solution. In this research, the viscosity value of sucrose solutions (aq) was extracted based on the known liquid density value, micropillar height, and the response of the QCM-P sensors using the developed hybrid model. In this study, all QCM-P sensors were systematically measured to extrapolate the viscosity values using the developed hybrid model. As an example, the comparison of measured viscosity values using square micropillar QCM-P (h_p = 18 μm) with reference values is shown in Table 2. It is clear that the values predicted by models are consistent with the reference viscosity values.

3.3. Damping and detection range analysis

The impedance spectra of QCM-P of square micropillars (h_p = 10 μm) operating in DI water and sucrose solutions with concentrations ranging from 0 to 40 wt% are illustrated in Fig. 12. It can be seen that as the concentration or viscosity of the sucrose increases, the resonance frequency f_0 of the QCM-P device decrease, and in the meantime, the bandwidth of the impedance signal increases which implies increased damping in the device.

Fig. 13 presents the impedance spectra of square and circular micropillar based QCM-P devices operating in DI water. As can be seen, when the micropillar height approaches the critical height (13.5 μm for square micropillar and 9.8 μm for circular micropillar) or reach the resonance points of the system, the HBW or damping increases.

The increase of damping can also be explained by modified Butterworth-Van Dyke (BVD) equivalent circuit [46,47] which is shown in Fig. 14 where the QCM is represented by three electrical components including L_q, C_q, and R_q, and the micropillar by L_p, C_p, and R_p. This is consistent with a two-degree-of-freedom model for QCM-P [32]. When micropillars are vibrating in liquids, the hydrodynamic loading on the pillars resulting in additional damping (ΔR_p) and mass loading (ΔL_p) (Fig. 16). In addition, the trapped liquid between the pillars can be

Table 2
Comparison of QCM-P measured viscosity vs. the Ref. value.

Concentration (wt %)	Ref. value viscosity (cP)	QCM-P measured viscosity (cP)	Absolute error (%)
10	1.186	1.249	5.3
20	1.727	1.829	5.9
30	2.831	2.774	2.0
40	5.474	5.356	2.2

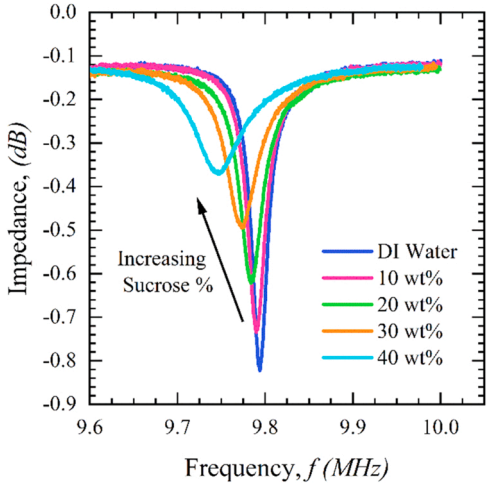

Fig. 12. Impedance spectra of square micropillar QCM-P (h_p = 10 μm) in sucrose solution (aq) with concentration ranging from 0 (DI water) to 40 wt%.

treated as classical viscous loading represented by L_f and R_f as described by Kanazawa et al. [22]. As a result, the damping of the QCM-P system will surely increase due to these effects. A quantitative analysis of the QCM-P damping based on modified BVD circuit is underway.

The limit of detection (LOD) of the QCM-P devices can be evaluated by:

$$\mathrm{LOD} = 3\frac{\mathrm{N}}{\mathrm{SE}}$$

where N (Hz) is the noise level of the frequency response of QCM devices operating in a blank solution (DI water) and SE is the sensitivity (Hz /wt %) of the device. The signal-to-noise ratio (SNR) of square micropillar based QCM-P (h_p = 11.5 μm) is shown in Fig. 15.

With the increase of sucrose concentration, the bandwidth of the impedance spectrum increases resulting in the increase of the noise level. However, the sensitivity enhancement due to micropillar structure exceeds the increase of the noise level. As a result, the QCM-P devices display a lower LOD in comparison to the traditional QCM/QCM-F devices. As the well-known minimum value of the SNR is around 10, the detection range of the QCM-P device (square micropillars at h_p = 11.5 μm) can be identified as from c = 0.21–40 wt%.

The induced hydrodynamic loading on micropillars is critical for

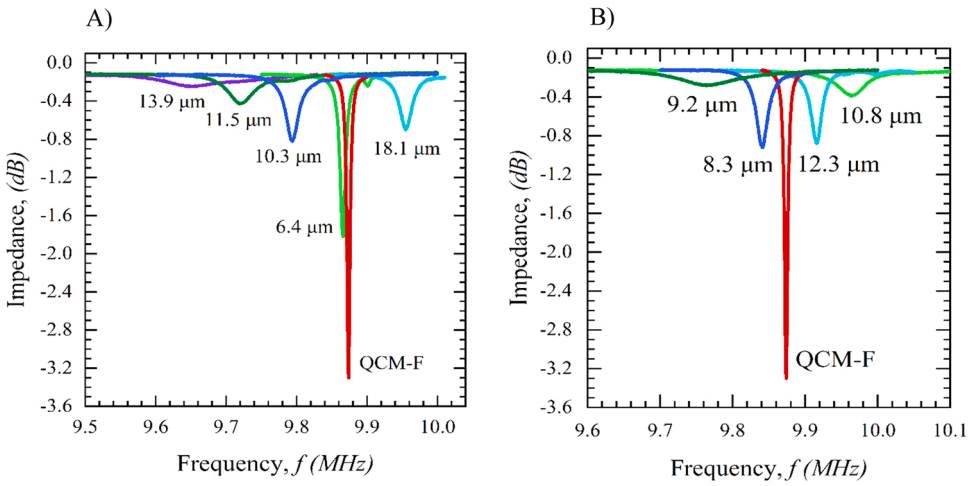

Fig. 13. Impedance spectrum of (A) squared micropillar and (B) circular micropillar based QCM-P devices operating in DI water.

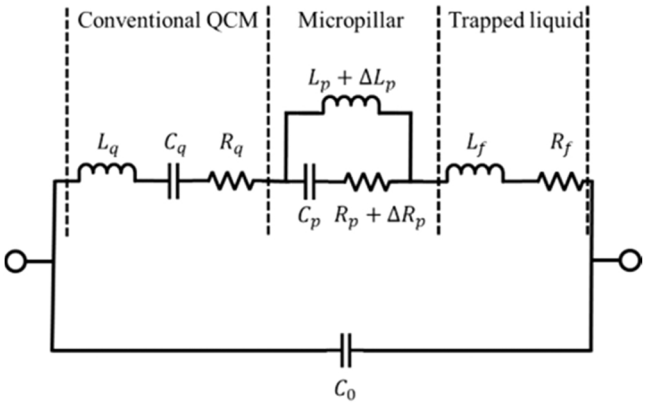

Fig. 14. Modified BVD equivalent circuit for QCM-P operating in a viscous liquid.

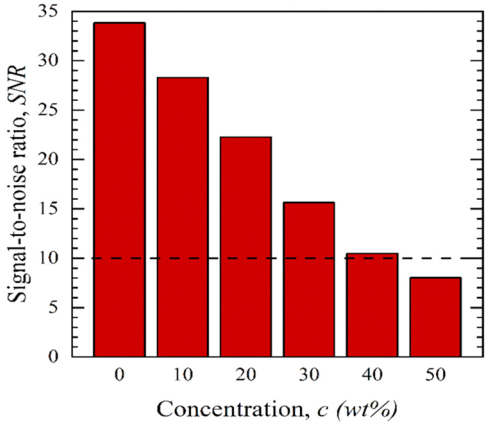

Fig. 15. Signal-to-noise ratio (SNR) of squared micropillar based QCM-P (h_p = 11.5 μm) in sucrose solutions.

understanding the dynamic response of QCM-P sensors operating in a liquid solution. The simulation results of the induced hydrodynamic loading are shown in Fig. 16. As h_p increases, the real part of induced hydrodynamic loading, $F_{hydro,real}$, increases until it reaches its maximum value at critical height. A sudden "jump and drop" of hydrodynamic loading can be observed due to the coupling between micropillars, solution, and QCM substrate. On the other side, a different trend is shown

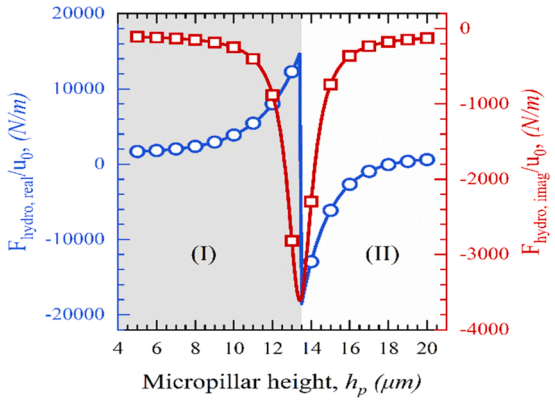

Fig. 16. Simulation results for induced hydrodynamic loading on the micropillar of square QCM-P in DI water.

for the imaginary part of the loading, $F_{hydro,imag}$, where it decreases as h_p increases. It reaches its minimum value at the critical height of the micropillar and then increases to a particular value before it decreases again. A comparison between Fig. 16 and Fig. 7A shows that the predicted critical height by hydrodynamic loading is consistent with the predicted f_0 and Γ of QCM-P sensors.

The "jump and drop" behavior in hydrodynamic loading is directly related to the phase shift angle (ϕ) between the coupled vibrations of micropillars and QCM substrate. When the micropillar height is smaller than critical height, the coupled vibration causes a $\phi < 90°$ (Stage I), the vibration of QCM is damped by the movement of the micropillars on its surface, resulting in an in-phase displacement of micropillar with quartz which causes an increase in the $F_{hydro,real}$. When the $\phi > 90°$, the phase veering occurs (Stage II), resulting in an out-phase displacement of micropillars with quartz, causing a sudden "jump and drop" behavior in the $F_{hydro,real}$.

4. Conclusion

This research focuses on the development of a novel micropillar-enhanced quartz crystal microbalance (QCM-P) device for viscosity measurement of a liquid droplet. A hybrid model based on the Krim-Holtz-Leedom-Matthaei equivalent circuit and numerical simulation was developed to analyze the dynamics of the QCM-P device and extract the viscosity of the liquid based on the liquid density, micropillar height, and the response of the QCM-P sensors. The results show that both the half bandwidth and resonance frequency of QCM-P can be utilized to

detect variations of liquid properties with different sensitivity levels depending on the micropillar's characteristics and solution properties. All the QCM-P sensors show significantly enhanced sensitivity in evaluating liquid viscosity compared to traditional QCM with the assistance of the hybrid model. The research demonstrates that the QCM-P device has great potential for droplet-based viscosity measurement applications. The signals of QCM-P were significantly damped when the micropillar height approaches the critical height. Therefore, future work will focus on the damping reduction of micropillars by optimizing the pillar geometry and modifying pillar surface properties such as hydrophobicity.

Declaration of Competing Interest

The authors declare that they have no known competing financial interests or personal relationships that could have appeared to influence the work reported in this paper.

Data availability

Data will be made available on request.

Acknowledgment

The authors thank MicroChem Corp. (Westborough, MA, USA) for providing PMMA material and financial support from National Science Foundation (NSF ECCS 2130716).

Appendix A. Supporting information

Supplementary data associated with this article can be found in the online version at doi:10.1016/j.sna.2022.114121.

References

[1] S. Zaccaron, K. Ahn, U. Henniges, A. Potthast, T. Rosenau, An improved, less erroneous protocol for the classical "cuen","cuoxam" or "cadoxen" viscosity measurements of pulps, Cellulose 29 (7) (2022) 3733–3744.
[2] D.K. Hameed, Engine oil deterioration based on the viscosity, flash point and fire point for different trip length, Kurd. J. Appl. Res. (2021) 13–20.
[3] T. Akyazi, L. Basabe-Desmonts, F. Benito-Lopez, Review on microfluidic paper-based analytical devices towards commercialisation, Anal. Chim. Acta 1001 (2018) 1–17.
[4] Z. Yan, Z. Li, S. Cheng, X. Wang, L. Zhang, L. Zheng, J. Zhang, From Newtonian to non-Newtonian fluid: insight into the impact of rheological characteristics on mineral deposition in urine collection and transportation, Sci. Total Environ. 823 (2022), 153532.
[5] E. Teko, K. Ako, A. Yousefi, C.D. Munialo, E. Osseyi, Rheological study of cowpea puree 'adowè'and the influence of saliva on the puree viscosity, Int. J. Food Sci. Technol. 57 (5) (2022) 3098–3105.
[6] S. Nazarian, N. Farsaeivahid, C. Grenier, D. Yunqing, M.L. Wang, Rapid electrochemical point-of-care COVID-19 detection in human saliva, Google Patents, 2021.
[7] E. Lee, B. Kim, S. Choi, Hand-held, automatic capillary viscometer for analysis of Newtonian and non-Newtonian fluids, Sens. Actuators A: Phys. 313 (2020), 112176.
[8] D.I. Sagdeev, V.F. I.g.R. Gabitov, M.G. Khairutdinov, V.A. Fomina, R.S. Alyaev, V. S. Sal'manov, F.M. Minkin, I.M. Gumerov, Abdulagatov, New design of the falling-body rheoviscometer for high and extra-high viscous liquid measurements. Viscosity of vacuum oils, J. Chem. Eng. Data 65 (4) (2020) 1773–1786.
[9] Y.J. Kim, B.-Y. Cho, S.-J. Lee, J. Hu, J.W. Wilde, Investigation of rheological properties of blended cement pastes using rotational viscometer and dynamic shear rheometer, Adv. Mater. Sci. Eng. (2018) (2018).
[10] H. Yabuno, Review of applications of self-excited oscillations to highly sensitive vibrational sensors, ZAMM-J. Appl. Math. Mech. /Z. für Angew. Math. und Mech. 101 (7) (2021), e201900009.
[11] S. Kurosawa, J.-W. Park, H. Aizawa, S.-I. Wakida, H. Tao, K. Ishihara, Quartz crystal microbalance immunosensors for environmental monitoring, Biosens. Bioelectron. 22 (4) (2006) 473–481.
[12] Y.-T. Xie, P. Chen, W.-Z. Wei, Rapid analysis of preservatives in beverages by ion chromatography with series piezoelectric quartz crystal as detector, Microchem. J. 61 (1) (1999) 58–68.
[13] D. Yu, B. Blankert, J.C. Viré, J.M. Kauffmann, Biosensors in drug discovery and drug analysis, Anal. Lett. 38 (11) (2005) 1687–1701.
[14] E. Benes, Improved quartz crystal microbalance technique, J. Appl. Phys. 56 (3) (1984) 608–626.
[15] A. Fort, A. Lo Grasso, M. Mugnaini, E. Panzardi, V. Vignoli, QCM measurements of RH with nanostructured carbon-based materials: Part 1 – theory and model, Chemosensors 10 (8) (2022) 315.
[16] D.A. Buttry, M.D. Ward, Measurement of interfacial processes at electrode surfaces with the electrochemical quartz crystal microbalance, Chem. Rev. 92 (6) (1992) 1355–1379.
[17] N.L. Torad, H. El-Hosainy, M. Esmat, K.E. El-Kelany, R. Tahawy, J. Na, Y. Ide, N. Fukata, W. Chaikittisilp, J.P. Hill, Phenyl-modified carbon nitride quantum nanoflakes for ultra-highly selective sensing of formic acid: a combined experimental by QCM and density functional theory study, ACS Appl. Mater. Interfaces 13 (41) (2021) 48595–48610.
[18] N.L. Torad, S. Zhang, W.A. Amer, M.M. Ayad, M. Kim, J. Kim, B. Ding, X. Zhang, T. Kimura, Y. Yamauchi, Advanced nanoporous material–based QCM devices: a new horizon of interfacial mass sensing technology, Adv. Mater. Interfaces 6 (20) (2019), 1900849.
[19] Y. Wang, C. Li, B. Zhao, Measurement of liquid viscosity using series resonant resistance response of quartz crystal microbalance, Jpn. J. Appl. Phys. 61 (4) (2022), 046503.
[20] L. Rodriguez-Pardo, J.F. Rodríguez, C. Gabrielli, H. Perrot, R. Brendel, Sensitivity, noise, and resolution in QCM sensors in liquid media, IEEE Sens. J. 5 (6) (2005) 1251–1257.
[21] W. Mason, Viscosity and shear elasticity measurements of liquids by means of shear vibrating crystals, J. Colloid Sci. 3 (2) (1948) 147–162.
[22] K.K. Kanazawa, J.G. Gordon, Frequency of a quartz microbalance in contact with liquid, Anal. Chem. 57 (8) (1985) 1770–1771.
[23] C. Stockbridge, Vacuum microbalance techniques. In: Proceedings of the Los Angeles Conference, 1966.
[24] H. Schilling, W. Pechhold, Two quartz resonator methods for the investigation of the complex shear modulus of polymers, Acta Acust. U. Acust. 22 (5) (1969) 244–253.
[25] S. Na Songkhla, T. Nakamoto, Interpretation of quartz crystal microbalance behavior with viscous film using a mason equivalent circuit, Chemosensors 9 (1) (2021) 9.
[26] S. Bruckenstein, M. Michalski, A. Fensore, Z. Li, A.R. Hillman, Dual quartz crystal microbalance oscillator circuit. Minimizing effects due to liquid viscosity, density, and temperature, Anal. Chem. 66 (11) (1994) 1847–1852.
[27] D. Johannsmann, W. Bucking, B. Bode, J. Petri, Simple frequency-based sensing of viscosity and dielectric properties of a liquid using acoustic resonators, IEEE Trans. Ultrason., Ferroelectr., Freq. Control 57 (3) (2010) 677–683.
[28] N. Doy, G. McHale, M. Newton, C. Hardacre, R. Ge, R. Allen, J. MacInnes, Separate density and viscosity determination of room temperature ionic liquids using dual quartz crystal microbalances, Sensors (2009) 287–290.
[29] F. Tan, D.-Y. Qiu, L.-P. Guo, P. Ye, H. Zeng, J. Jiang, Y. Tang, Y.-C. Zhang, Separate density and viscosity measurements of unknown liquid using quartz crystal microbalance, AIP Adv. 6 (9) (2016), 095313.
[30] P. Wang, J. Su, W. Dai, G. Cernigliaro, H. Sun, Ultrasensitive quartz crystal microbalance enabled by micropillar structure, Appl. Phys. Lett. 104 (4) (2014), 043504.
[31] P. Wang, J. Su, C.-F. Su, W. Dai, G. Cernigliaro, H. Sun, An ultrasensitive quartz crystal microbalance-micropillars based sensor for humidity detection, J. Appl. Phys. 115 (22) (2014), 224501.
[32] J. Su, H. Esmaeilzadeh, F. Zhang, Q. Yu, G. Cernigliaro, J. Xu, H. Sun, An ultrasensitive micropillar-based quartz crystal microbalance device for real-time measurement of protein immobilization and protein-protein interaction, Biosens. Bioelectron. 99 (2018) 325–331.
[33] S. Ji, H. Esmaeilzadeh, J. Su, S. Pagsuyoin, H. Sun, Novel analysis of a micropillar coupled acoustic wave sensor, Sens. Actuators Rep. 3 (2021), 100034.
[34] J.E. Sader, Frequency response of cantilever beams immersed in viscous fluids with applications to the atomic force microscope, J. Appl. Phys. 84 (1) (1998) 64–76.
[35] H. Esmaeilzadeh, J. Su, S. Ji, G. Cernigliaro, F.K. Gehring, H. Sun, Lowest detectable protein immobilization measurement using an ultrasensitive micropillar-based quartz crystal microbalance (QCM-P) device, IEEE Sens. J. 19 (21) (2019) 9672–9679.
[36] J. Su, H. Esmaeilzadeh, P. Wang, S. Ji, M. Inalpolat, M. Charmchi, H. Sun, Effect of wetting states on frequency response of a micropillar-based quartz crystal microbalance, Sens. Actuators A: Phys. 286 (2019) 115–122.
[37] A. Arnau, Piezoelectric Transducers and Applications, Springer, 2004.
[38] W.P. Mason, Physical acoustics and the properties of solids, van Nostrand1958.
[39] A. Arnau, A review of interface electronic systems for AT-cut quartz crystal microbalance applications in liquids, Sensors 8 (1) (2008) 370–411.
[40] R. Krimholtz, D.A. Leedom, G.L. Matthaei, New equivalent circuits for elementary piezoelectric transducers, Electron. Lett. 6 (13) (1970) 398–399.
[41] X. Xie, J. Xie, W. Luo, Z. Wu, Electromechanical coupling and frequency characteristics of a quartz crystal resonator covered with micropillars, J. Vib. Acoust. 141 (4) (2019).
[42] P. Wang, J. Su, L. Gong, M. Shen, M. Ruths, H. Sun, Numerical simulation and experimental study of resonance characteristics of QCM-P devices operating in liquid and their application in biological detection, Sens. Actuators B: Chem. 220 (2015) 1320–1327.
[43] A. Kierkegaard, S. Boij, G. Efraimsson, A frequency domain linearized Navier–Stokes equations approach to acoustic propagation in flow ducts with sharp edges, J. Acoust. Soc. Am. 127 (2) (2010) 710–719.
[44] A. Kierkegaard, S. Boij, G. Efraimsson, Simulations of the scattering of sound waves at a sudden area expansion, J. Sound Vib. 331 (5) (2012) 1068–1083.

[45] M.J. Herring Jensen, E. Svensson, K. Shaposhnikov, Using the linearized Navier-Stokes equations to model acoustic liners, In: Proceedings of the 2018 AIAA/CEAS Aeroacoustics Conference, 2018, p. 3783.
[46] S. Butterworth, On electrically-maintained vibrations, Proc. Phys. Soc. Lond. 27 (1) (1914) 410.
[47] K.S. Van Dyke, The piezo-electric resonator and its equivalent network, Proc. Inst. Radio Eng. 16 (6) (1928) 742–764.

Mr. Ilia Chiniforooshan Esfahani received a B.S. degree in mechanical engineering from Sharif University of Technology (SUT) and joined Northeastern University (NEU) to pursue his Ph.D. in mechanical engineering. His Ph.D. research is related to the experimental and computational investigation of fluid/surface interaction, focusing on the viscosity effect. His research interests include biosensor development, computational fluid dynamics, and MEMS.

Prof. Hongwei Sun Joined Mechanical and Industrial Engineering department at Northeastern University (NEU) in September 2020. His research interests include multiphase thermal transport phenomena, acoustic wave bio and chemical sensors and actuators, thermal management of fibers and films, thermal energy storage materials and processing, microchannel cooling systems, nanoimprinting process and applications, MEMS/NEMS fabrication, microfluidics and bioMEMS; nanoscale magnetic assembly and applications. Prior to joining Northeastern, Prof. Sun was a full professor in the Mechanical Engineering department at University of Massachusetts Lowell (UML) where he started his career as an assistant professor in 2005. He held a postdoctoral fellow position at University of Rhode Island between 1998 and 2001 and then became a research scientist with tenure at Massachusetts Institute of Technology (MIT). Prof. Sun is an author of more than 80 peer-reviewed publications and national/international patents. He has served as a board member of several committees such as NSF PIER Advisory Board (2008–2009) and MEMS/NMES Workshops and has been serving as the organizer of ASME IMECE Micro/Nanofluidic symposium (2015–2018). Prof. Sun is a recipient of Entrepreneurial Faculty Award in 2016.